



## Low-spin, mononuclear, Fe(III) complexes with P,N donor hemilabile ligands: A combined experimental and theoretical study

Pankaj Das<sup>a,\*</sup>, Podma Pollov Sarmah<sup>a</sup>, Malabika Borah<sup>a</sup>, Ashwini K. Phukan<sup>b,\*</sup>

<sup>a</sup> Department of Chemistry, Dibrugarh University, Dibrugarh 786 004, Assam, India

<sup>b</sup> Department of Chemical Sciences, Tezpur University, Napaam, Assam, India

### ARTICLE INFO

#### Article history:

Received 18 February 2009

Received in revised form 23 July 2009

Accepted 3 August 2009

Available online 8 August 2009

#### Keywords:

Fe(III) complexes

Low-spin

Hemilabile ligand

Magnetic study

DFT calculation

### ABSTRACT

Two new mononuclear Fe(III) complexes,  $[\text{FeCl}_3\{\text{PPh}_2(p\text{-C}_6\text{H}_4\text{NMe}_2)\text{-P}\}_3](\mathbf{1})$  ( $\text{PPh}_2(p\text{-C}_6\text{H}_4\text{NMe}_2)$ : 4-(dimethylamino)phenyldiphenylphosphine) and  $[\text{FeCl}_3(\text{PPh}_2\text{py-P})(\text{PPh}_2\text{py-P,N})](\mathbf{2})$  ( $\text{PPh}_2\text{py}$ : diphenyl(2-pyridyl)phosphine) were synthesized by reacting anhydrous  $\text{FeCl}_3$  with respective ligand in acetonitrile solution under refluxing condition. Both the complexes were characterized by elemental analysis, FAB-Mass, FTIR, UV-Vis, ESR, Cyclic Voltammetry and magnetic measurement. The FAB mass spectra of complexes  $\mathbf{1}$  and  $\mathbf{2}$  show molecular ion peak at  $m/z$  1078  $[\text{M}]^+$  and  $m/z$  687  $[\text{M}-1]^+$ , respectively, indicating mononuclear nature of the complexes. UV-Vis spectra of the complexes were consistent with low-spin, octahedral geometry. The variable temperature magnetic susceptibility measurement (73–323 K) of these complexes is also consistent with the paramagnetic nature of the complexes with a ground state spin  $S = 1/2$ . The Fe(III) centers of these two complexes remain low-spin, both at room temperature and liquid nitrogen temperature, was also indicated by the ESR analysis. Cyclic Voltammetry of both the complexes show an irreversible oxidation wave attributed to  $\text{Fe}^{3+} \rightarrow \text{Fe}^{4+} + e^-$  along with the peak for ligand oxidation. Theoretical calculations (B3LYP) of the complexes show that for complex  $\mathbf{1}$ , a *trans* geometry of the two phosphorous atoms and for complex  $\mathbf{2}$ , a *mer,cis* structures are the most favored geometrical isomer. TDDFT calculations were performed to interpret the observed bands in the UV-Visible spectra.

© 2009 Elsevier B.V. All rights reserved.

### 1. Introduction

The chemistry of mononuclear Fe(III) complexes with mixed donor ligands, particularly, where one of the donor atom is nitrogen, have gained much attention because such type of complexes could mimic the active site of several non-heme metalloproteins. During the last two decades, several bio-inspired Fe(III) complexes were reported [1–15] with different N,O [6,7]/N,S [1–5]/N,N [8–15] donor ligands which serve as synthetic model for the active site of different non-heme metalloenzymes e.g., Fe(III) complexes of (i) N,N donors ligands were used as models for the catechol dioxygenases [8–10], the enzyme responsible for the cleavage of C–C bonds between the two hydroxyl groups of catechol, (ii) N,S donor ligands were used as model for nitrile hydratase [1–5], the enzyme responsible for the conversion of nitrile to corresponding amide, (iii) N,O donor ligands were used as model for the iron oxygenases, the enzyme responsible for alkane and alkene oxidation, etc. Though, a large number synthetic models of these enzymes were reported but only few of them were found to be successful as functional

model. It is worthy to note here that the majority of the reported Fe(III) complexes with such mixed donor ligands are either high spin [6,8,9,13,16,17] with  $S = 5/2$  or exhibit spin equilibria [1–3,5] between  $S = 5/2 \leftrightarrow S = 1/2$  but, the Fe(III) center in most of these enzymes remain mostly low-spin [2,18]. Thus, there has been considerable interest in the synthesis of Fe(III) complexes with a ligand system that could stabilize the metal in low-spin state, as, such ligands are expected to bring the electronic property of the metal center comparable to the biological system. In addition, it is also known from literature that for the complexes to act as functional model, it is highly desired that the complexes should have a vacant coordination site or a labile ligand which could be easily replaced by an incoming substrate [19,20]. Thus, we were intrigued by the possibility that introduction of a bifunctional P,N donor ligand, so-called “hemilabile ligand”, which have two different donor functionalities within the same molecule, i.e., the substitutionally inert P atom (due to  $d\pi\text{-}p\pi$  back bonding) and substitutionally labile N atom, could perform a dual role, in which, the phosphine donor could stabilize the metal in low-spin state [21] while the nitrogen donor might create a vacant site for substrate binding by opening the chelate without complete detachment of the ligand from the molecule (Chart 1). Because of this unique property, such type of ligands got considerable application in homogeneous catalysis particularly by late transition metals.

\* Corresponding authors. Tel.: +91 9435394373; fax: +91 3732370323 (P. Das).  
E-mail addresses: [pankajd29@yahoo.com](mailto:pankajd29@yahoo.com) (P. Das), [ashwini@tezu.ernet.in](mailto:ashwini@tezu.ernet.in) (A.K. Phukan).



Chart 1. Creation of a vacant coordination site by hemilabile ligand.

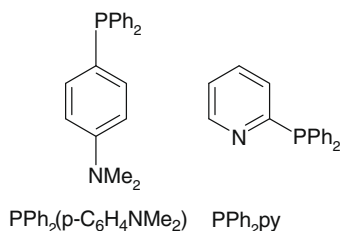


Chart 2. P, N, donors ligands.

As part of our interest on the coordination chemistry of iron with mixed P,N donor ligand [22], in this work, we report syntheses of two mononuclear Fe(III) complexes with two P,N donor ligands (Chart 2). Among the two ligands, the diphenyl(2-pyridyl)phosphine is one of the most extensively used phosphine ligands applied in coordination chemistry and four different bonding modes of this ligand were reported in literature [23]: P-monodentate, N-monodentate, P–N bridge and P–N chelated modes. This ligand has previously been employed in the synthesis of some iron complexes [24–27] with 0 and +2 oxidation state, though, there is no report on Fe(III) complexes. On the other hand, the coordination chemistry of the aminophosphine ligand, PPh<sub>2</sub>(*p*-C<sub>6</sub>H<sub>4</sub>NMe<sub>2</sub>), is relatively unknown and to the best of our knowledge, there is no report on complexes of this ligand with Fe atom in any of its oxidation states. It is noteworthy to mention here that Fe(III) complexes with phosphine based ligands are relatively less common may be due to the soft nature of phosphorous could not stabilize a hard Fe(III) center. Moreover, the steric property of the substituent on the phosphorous atom of such ligands is known to play a dominant role in determining the coordination geometry of the metal complexes, particularly for iron [28] and ruthenium [29]. The complexes **1** and **2** were characterized by different experimental techniques. Further, DFT calculations were performed to find the most stable geometrical isomer of **1** and **2** as well as to interpret their UV–Vis spectra.

## 2. Experimental

### 2.1. Materials

The ligands 4-(dimethylamino)phenyldiphenylphosphine and diphenyl(2-pyridyl)phosphine were purchased from Aldrich. Anhydrous FeCl<sub>3</sub> and other necessary chemicals were purchased from RENKEM, India. The solvents used are of analytical grade and distilled prior to utilization. All the reactions were carried out under N<sub>2</sub> atmosphere.

### 2.2. Synthesis

#### 2.2.1. Synthesis of complex [FeCl<sub>3</sub>{PPh<sub>2</sub>(*p*-C<sub>6</sub>H<sub>4</sub>NMe<sub>2</sub>)-P}<sub>3</sub>] (**1**)

A solution of the ligand PPh<sub>2</sub>(*p*-C<sub>6</sub>H<sub>4</sub>NMe<sub>2</sub>) (0.20 g, 0.66 mmol) in 50 ml of acetonitrile was added drop by drop to a solution of anhydrous FeCl<sub>3</sub> (0.036 g, 0.22 mmol) in 50 ml acetonitrile. The reaction mixture was refluxed under nitrogen for 1 hour. The color of the solution changed gradually from yellow (FeCl<sub>3</sub> in acetonitrile) to dark brown color. After cooling the reaction mixture, the solvent was evaporated and the resultant solid mass was washed

several times with ether and hexane. Finally, after drying under vacuum, a dark brown compound was obtained which was recrystallized from acetonitrile. Yield: 86%.

*Anal. Calc.* for C<sub>60</sub>H<sub>60</sub>N<sub>3</sub>P<sub>3</sub>Cl<sub>3</sub>Fe: C, 66.83; H, 5.60; N, 3.89. Found: C, 66.36; H, 5.55; N, 3.84%. MS-FAB *m/z* (%): 1078 (5), [M]<sup>+</sup>; [FeCl<sub>3</sub>{PPh<sub>2</sub>(*p*-C<sub>6</sub>H<sub>4</sub>NMe<sub>2</sub>)<sub>3</sub>}]<sup>+</sup>; 1050 (30), [M–2Me+2]<sup>+</sup>; [FeCl<sub>3</sub>{PPh<sub>2</sub>(*p*-C<sub>6</sub>H<sub>4</sub>N)+2H]<sup>+</sup>; 1034 (25), [M–NMe<sub>2</sub>]<sup>+</sup>; [FeCl<sub>3</sub>{PPh<sub>2</sub>(*p*-C<sub>6</sub>H<sub>4</sub>)}]<sup>+</sup>; 1042 (20), [M–Cl–1]<sup>+</sup>; [FeCl<sub>2</sub>{PPh<sub>2</sub>(*p*-C<sub>6</sub>H<sub>4</sub>NMe<sub>2</sub>)<sub>3</sub>-H]<sup>+</sup>; 1005 (20), [M–2Cl–2]<sup>+</sup>; [FeCl{PPh<sub>2</sub>(*p*-C<sub>6</sub>H<sub>4</sub>NMe<sub>2</sub>)<sub>3</sub>-2H]<sup>+</sup>. Selected IR frequencies (cm<sup>-1</sup>, KBr): 3062 (ν<sub>CH</sub>), 1482 (ν<sub>C=C</sub>), 1439 (ν<sub>C=C</sub>), 1374 (ν<sub>C-N</sub>), 1129 (ν<sub>PC</sub>), 1071 (ν<sub>PC</sub>), 544 (ν<sub>FeP</sub>); Far IR (Nujol): 337(ν<sub>Fe-Cl</sub>), 310 (ν<sub>Fe-Cl</sub>), 282(ν<sub>Fe-Cl</sub>). UV–Vis (CH<sub>3</sub>CN), λ<sub>max</sub> (nm): 352, 503. ESR: *g* = 2.01(RT), 2.00 (LNT). CV (CH<sub>3</sub>CN): *E*<sub>pa</sub>: 0.518 V, 1.072 V; *E*<sub>pc</sub>: -0.114 V; Δ*E*<sub>p</sub> = 632 mV; *E*<sub>1/2</sub> = 0.316 V.

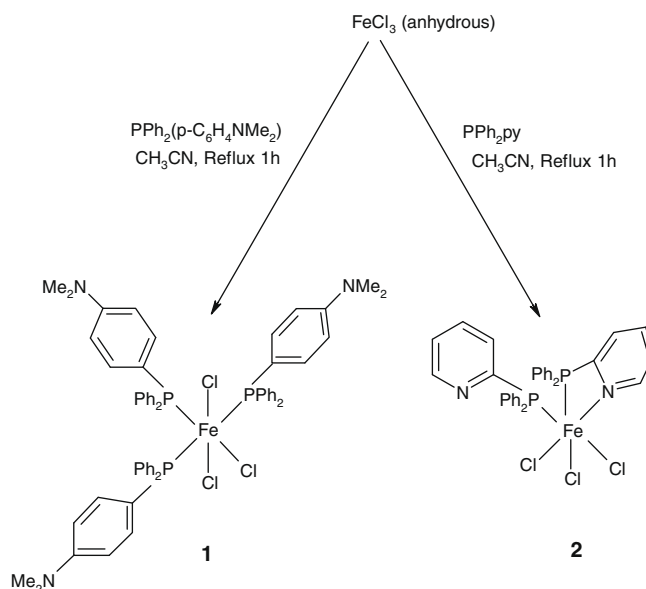
#### 2.2.2. Synthesis of [FeCl<sub>3</sub>(PPh<sub>2</sub>py-P)(PPh<sub>2</sub>py-P,N)<sub>2</sub>](**2**)

The complex **2** was prepared by following a similar procedure of complex **1**, using the ligand PPh<sub>2</sub>py (0.18 g, 0.66 mmol) and anhydrous FeCl<sub>3</sub> (0.036 g, 0.22 mmol). During refluxing, the color of the solution changed gradually from yellow to light brown. After thorough washing with ether and hexane, a yellowish brown compound was obtained which was recrystallized from acetone. Yield: 85%.

*Anal. Calc.* for C<sub>34</sub>H<sub>28</sub>N<sub>2</sub>P<sub>2</sub>Cl<sub>3</sub>Fe: C, 59.26; H, 4.07; N, 4.07. Found: C, 58.96; H, 4.05; N, 4.05%. (data are calculated on MW 688.5 however if MW changed then C, H, N value will be changed). MS-FAB *m/z* (%): 687 (10), [M–1]<sup>+</sup>; [FeCl<sub>3</sub>(PPh<sub>2</sub>py)<sub>2</sub>-H]<sup>+</sup>; 651 (90), [M–Cl–2]<sup>+</sup> [[FeCl<sub>2</sub>(PPh<sub>2</sub>py)<sub>2</sub>-2H]<sup>+</sup>; selected IR frequencies (cm<sup>-1</sup>, KBr): 3056 (ν<sub>CH</sub>), 1602 (ν<sub>C=N</sub>), 1588 (ν<sub>C=N</sub>), 1481 (ν<sub>C=C</sub>), 1435 (ν<sub>C=C</sub>), 1122 (ν<sub>PC</sub>), 1067 (ν<sub>PC</sub>), 557 (ν<sub>FeP</sub>), 537 (ν<sub>FeP</sub>); Far IR, (Nujol): 360 (ν<sub>Fe-Cl</sub>), 330 (ν<sub>Fe-Cl</sub>), 279 (ν<sub>Fe-Cl</sub>) 254 (ν<sub>Fe-N</sub>). UV–Vis (CH<sub>3</sub>CN), λ<sub>max</sub> (nm): 228, 297, 403, 526; ESR: *g* = 2.04 (RT), 2.02 (LNT). CV (CH<sub>3</sub>CN): *E*<sub>pa</sub>: 0.116 V, 1.159 V; *E*<sub>pc</sub>: -0.097 V; Δ*E*<sub>p</sub> = 212 mV; *E*<sub>1/2</sub> = 0.106 V.

### 2.3. Physical measurements

IR spectra (4000–400 cm<sup>-1</sup>) were recorded on Nicolet Impact 410 spectrophotometer in KBr medium and Far IR spectra were recorded on Perkin–Elmer 883 spectrophotometer using Nujol. The



Scheme 1. Synthesis of complexes **1** and **2**.

UV–Vis spectra were recorded in acetonitrile solution [ca.  $1.0 \times 10^{-4}$  M] in  $1 \text{ cm}^3$  cell in the range 200–800 nm using a Shimadzu, Graphicord UV-240 spectrophotometer. Elemental analysis (C, H and N) were done on Perkin–Elmer 2400 elemental analyzer. The FAB mass spectra were recorded on a JEOL SX 102/DA-6000 Mass spectrometer/data system using argon (6 kV, 10 mA) as the FAB gas and m-nitrobenzylalcohol was used as the matrix. The accelerating voltage was 10 kV and the spectra were recorded at room temperature. The ESR spectra were recorded in solid state as well as at liquid nitrogen temperature using tetracyanoethylene (TCNE) as reference by using Varian, E-112 spectrometer. Magnetic measurements were performed using ADE DMS Vibrating Sample Magnetometer, Model EV 7, USA and the diamagnetic corrections were made using Pascal's constant. The effective magnetic moments ( $\mu_{\text{eff}}$ ) were calculated from the equation,  $\mu_{\text{eff}} = 2.83(\chi_{\text{M}}T)^{1/2}$  (BM). Cyclic voltammetric study of the complexes were recorded in acetonitrile solution with a CH Instruments, Model 600C using Pt as working electrode and Ag/AgCl as the reference electrode with tetrabutylammoniumperchlorate (TBAP) as the supporting electrolyte.

### 3. Computational details

All the structures were completely optimized using the hybrid HF-DFT method, labeled as B3LYP [30–32] without any symmetry constraint. This is based on Becke's three-parameter functional [30] including Hartree–Fock exchange contribution with a non-local correction for the exchange potential proposed by Becke [31] together with the non-local correction for the correlation energy suggested by Lee et al. [32]. We have used the LANL2DZ basis set with the effective core potentials (ECP) of Hay and Wadt [33–35] for the metal atoms and 6-31+G\* basis set for other atoms as implemented in the GAUSSIAN 03 suite of programs [36]. The structures were further confirmed as real minima by running analytical vibrational frequency calculations at the same level of theory. For compound **1**, the  $\text{PPh}_2\text{C}_6\text{H}_4\text{NMe}_2$  group was modeled initially by  $\text{PH}_3$  group for both Fe and Ru. However, modeling by the more realistic  $\text{PH}_2\text{C}_6\text{H}_4\text{NH}_2$  group, in which the two bulky phenyl groups were replaced by two hydrogen atoms, was carried out only for the iron complexes. Compound **2** was modeled by replacing the phenyl groups with hydrogen atoms. Further, time dependent DFT

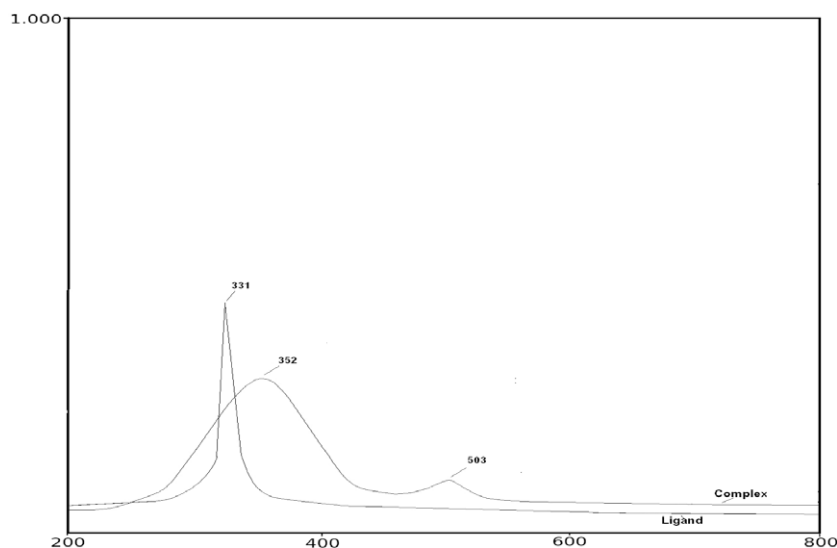


Fig. 1. UV–Vis spectra of complex **1** recorded in  $1.0 \times 10^{-4}$  M acetonitrile solution.

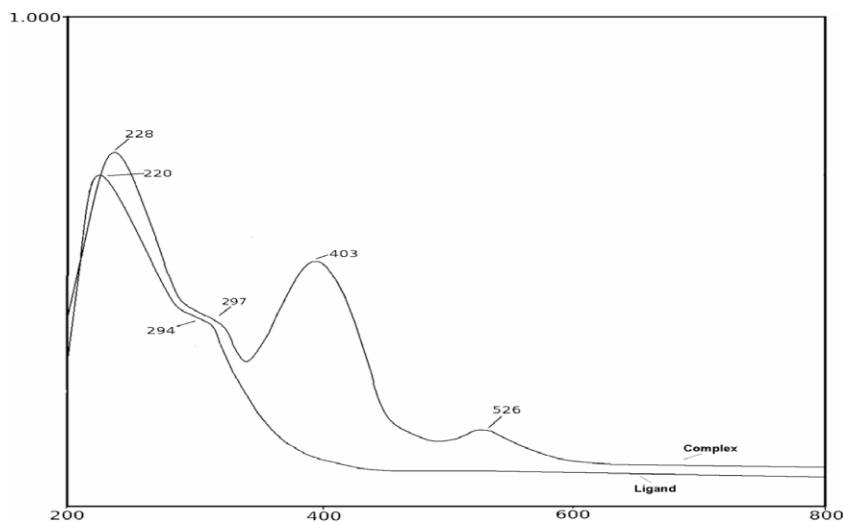


Fig. 2. UV–Vis spectra of complex **2** recorded in  $1.0 \times 10^{-4}$  M acetonitrile solution.

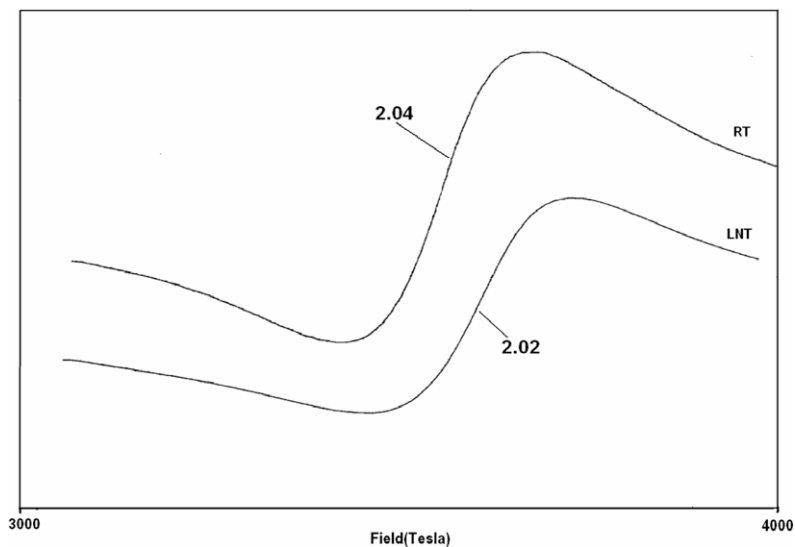


Fig. 3. The solid state ESR spectra of complex **1** recorded at room temperature (RT) and liquid nitrogen temperature (LNT).

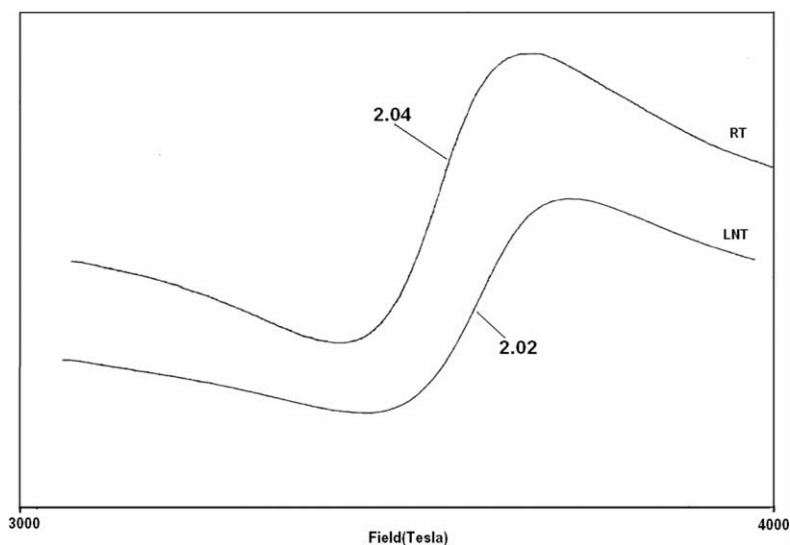


Fig. 4. The solid state ESR spectra of complex **2** recorded at room temperature (RT) and liquid nitrogen temperature (LNT).

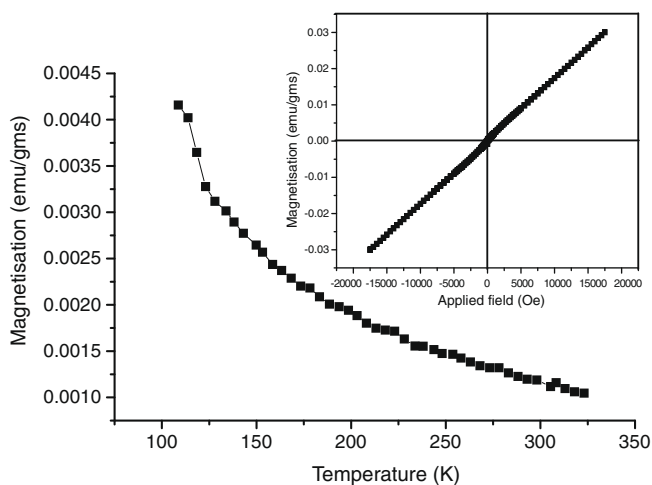


Fig. 5. Variable Temperature (73–323 K) magnetic susceptibility measurement curve ( $\chi_g$  vs.  $T$ ) of complex **1** (field 1000 Oe).

(TDDFT) calculations were performed on the minimum energy structure of **1** and **2** to assign the observed electronic transitions in the UV–Vis spectra [37–39].

## 4. Results and discussion

### 4.1. Synthesis of complexes

The reaction of three molar equivalent of the  $\text{PPh}_2(p\text{-C}_6\text{H}_4\text{NMe}_2)$  ligand with one molar equivalent of anhydrous  $\text{FeCl}_3$  in acetonitrile solution under refluxing condition for 1 hour gave complex  $[\text{FeCl}_3\{\text{PPh}_2(p\text{-C}_6\text{H}_4\text{NMe}_2)\text{-P}\}_3]$  (**1**) (Scheme 1) as dark brown solid. On the other hand, the reaction of two molar equivalent of the ligand  $\text{PPh}_2\text{Py}$  with one molar equivalent of anhydrous  $\text{FeCl}_3$  in acetonitrile solution under refluxing condition for 1 hour yield a bright yellow compound  $[\text{FeCl}_3(\text{PPh}_2\text{py-P})(\text{PPh}_2\text{py-P,N})_2]$  (**2**). It might be important to note here that we have also tried to synthesis an analogous stoichiometric complex of **1** by using three molar equivalent

of the ligand PPh<sub>2</sub>py with one molar equivalent of the FeCl<sub>3</sub>, but, only the complex **2** was isolated as final product. The synthesis of complexes **1** and **2** from two bulky phosphine ligands are in clear contrast with the observations of Walker and Poli [28], where, they found that the interaction of FeCl<sub>3</sub> with phosphines resulted an octahedral complex when a less bulky ligand such as Me<sub>3</sub>P was used while, a tetra- or penta-coordinated complexes was formed when a more bulky ligand like PPh<sub>3</sub> was used. However, Dilworth et al. [40] had synthesized a series of Fe(III) complexes as their hexafluorophosphate/tetraphenylborate salts from FeCl<sub>3</sub> with some sterically crowded functionalized phosphine ligands where they found that the Fe(III) complexes are octahedral in nature. The elemental analysis (C, H, N) and FAB mass spectra of the complexes **1** and **2** are in clear agreement with the above formulation. The FAB mass spectra of complex **1** shows a very less intense molecular ion peak at *m/z* 1078 [M]<sup>+</sup> along with two other prominent peaks at *m/z* 1042 and *m/z* 1005 corresponding to [M–Cl–1]<sup>+</sup> and [M–2Cl–2]<sup>+</sup> ions, respectively, indicating mononuclear nature of the complex. The complex **2** also shows a very less intense molecular ion peaks at *m/z* 687 [M–1]<sup>+</sup> along with a high intense peak (90%) at *m/z* 651 for [M–Cl–2]<sup>+</sup> which is consistent with mononuclear nature of the complex. Attempts to obtain diffraction-quality crystals for both the complexes, using different combination of solvents, were unsuccessful. We noticed some side reactions (as indicated by the change in color of the solution) that made the complexes unstable in solution during the long delay necessary for good crystallization. Both the complexes **1** and **2** are stable in solid state but gradually decompose in solution.

#### 4.2. Infrared spectra

For ligands containing tertiary amine or pyridyl groups, the analysis of the IR spectra indicates whether they are coordinated or not, by observing the changes in the frequency of the  $\nu_{\text{amine}}(\text{C-N})$  or  $\nu_{\text{py}}(\text{C=N})$  stretching. The complex **1** shows  $\nu_{\text{amine}}(\text{C-N})$  stretching at 1375 cm<sup>-1</sup> which is almost equal to the  $\nu_{\text{amine}}(\text{C-N})$  value of the free ligand indicating monodentate nature of the phosphinoamine ligand. In addition to other characteristics band of the free ligands, the complex **1** also show a new band at 544 cm<sup>-1</sup> which is the characteristics region of M–P stretching [41]. The Far IR spectrum of the complex **1** show three stretching frequencies for  $\nu(\text{Fe-Cl})$  at 337, 310 and 282 cm<sup>-1</sup> indicating *mer* arrangement [23] of the chloride. In the case of phosphinopyridine ligand, the coordination of N atom of the PPh<sub>2</sub>py to a metal ion is expected to shift the  $\nu(\text{C=N})$  bands of pyridine to higher frequencies [23]. The complex **2** shows two weak bands at 1602 and 1588 cm<sup>-1</sup> which are attributed to the  $\nu(\text{C=N})$  vibrations of N-coordinated and non-coordinated phosphino pyridines, respectively. The coordination of the pyridyl nitrogen group was also indicated by the presence of a band at 254 cm<sup>-1</sup> in the Far IR region which is assigned to the  $\nu(\text{Fe-N})$  stretching [42]. The Far IR spectrum also shows three  $\nu(\text{Fe-Cl})$  bands at 360, 330 and 279 cm<sup>-1</sup> indicating a *mer* arrangement of chlorides [23]. Recently Hermanowicz et al. [23] have reported two phosphinopyridine complexes, [MCl<sub>3</sub>(PPh<sub>2</sub>py-P)(PPh<sub>2</sub>py-P,N)<sub>2</sub>] (M = Rh and Ru), for which X-ray structural investigation shows that the complexes were mononuclear *mer,cis* isomer with monodentate and bidentate pyridyl phosphine ligands.

#### 4.3. UV-Vis spectra

The UV-Vis spectrum of the complexes **1** and **2** along with their respective ligands are shown in Figs. 1 and 2, respectively. The spectra of the complex **1** in acetonitrile show one intense absorption band at 352 nm assigned to intraligand *n-π\** transition and compared to the free ligand (331 nm), this band shifted towards

red indicating change of the electronic environment of the ligand due to complexation. The complex **1** also show a low energy band at 503 nm attributed to the LMCT absorptions due to phosphine-Fe<sup>3+</sup>(3d) transition with some contribution from the coordinated chloride. The UV-Vis spectrum of the complex **2** in acetonitrile exhibits one intense band at 228 nm and a shoulder at 297 nm which could be attributed to the intraligand *π-π\** and *n-π\** transitions [11,23], respectively. Compared to the free ligand (220 nm and 294 nm), these bands shifted towards red, and is consistent with change in electronic environment of the ligand due to complex formation. In addition to the ligand centered bands, the complex **2** also show two other bands at 403 nm and at 526 nm which may be attributed to LMCT absorptions. The absorption bands of the phosphinopyridine complex **2** are quite similar to those found for other pyridine based low-spin Fe(III) complexes [11].

#### 4.4. ESR spectra

The ESR spectra of the both the complexes **1** and **2** were recorded in solid state at liquid nitrogen temperature and also at room temperature. The spectra were represented in Figs. 3 and 4, respectively. The spectrum of **1**, both at RT and LNT exhibit a broad signal with a *g* value of 2.01 and 2.00, respectively, consistent with a regular octahedral symmetry with low-spin d<sup>5</sup> Fe(III) system [1,14]. Similar to complex **1**, the complex **2** also show a broad signal with a *g* value of 2.04 and 2.02 indicating low-spin octahedral geometry of the Fe(III) complex.

#### 4.5. Magnetic study

The magnetic susceptibility ( $\chi_g$ ) data for the powder sample of the complexes **1** and **2** were collected in the temperature range of

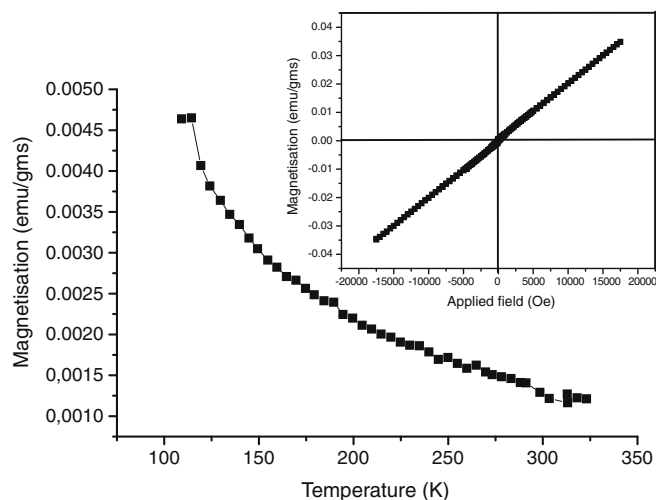


Fig. 6. Variable Temperature (73–323 K) magnetic susceptibility measurement curve of complex **2** (field 1000 Oe).

Table 1

Temperature,  $\chi_{MT}$  (in emu K mol<sup>-1</sup>) and magnetic moment.

Complex 1			Complex 2		
Temperature (T in K)	$\chi_{MT}$	$\mu_{\text{eff}}$ (BM)	Temperature (T)	$\chi_{MT}$	$\mu_{\text{eff}}$ (BM)
123	0.43	1.86	123	0.32	1.60
173	0.42	1.82	173	0.31	1.58
223	0.41	1.81	223	0.29	1.53
273	0.40	1.79	273	0.28	1.51
323	0.39	1.76	323	0.28	1.50

73–323 K in an applied magnetic field of 1000 Oe. The plot of  $\chi_g$  versus  $T$  of the complexes **1** and **2** were represented in Figs. 5 and 6, respectively. The temperature dependant magnetic susceptibility of both the complexes show a decrease in susceptibility with increasing temperature, and the field dependence susceptibility at room temperature show a strictly linear behavior with no hysteresis phenomena clearly indicating paramagnetic nature of the complexes. As the iron(III) system has a  $3d^5$  configuration, it's complex may be either high spin ( $S = 5/2$ ) or low-spin ( $S = 1/2$ ). However, the effective magnetic moment ( $\mu_{\text{eff}}$ ) measurements of the complexes at different temperature (Table 1) are in the range of 1.5–1.9 BM and is consistent with the low-spin nature of both the complexes.

#### 4.6. Cyclic voltammetry

The electrochemical behavior of the complexes **1** and **2** were studied by Cyclic Voltammetry in acetonitrile using 0.1 M TBAP as the supporting electrolyte and the voltgrams are presented in the supplementary materials (Figs. S1 and S2). It has been demonstrated that complex **1** exhibits an one electron redox process at  $E_{1/2} = 0.316$  V attributable to  $\text{Fe}^{\text{III}} \rightarrow \text{Fe}^{\text{IV}} + e^-$ , redox system and the process is chemically as well as electrochemically irreversible as indicated by  $i_{\text{pc}}/i_{\text{pa}} \neq 1$  and extremely high  $\Delta E_p$  value of 632 mV. In addition, the complex **1** also show another oxidation peak at 1.072 V attributed to the irreversible ligand oxidation. Similar to complex **1**, the complex **2** also exhibit an irreversible redox couple for  $\text{Fe}^{\text{III}}/\text{Fe}^{\text{IV}}$  oxidation at  $E_{1/2} = 0.106$  V with  $\Delta E_p$  of 212 mV

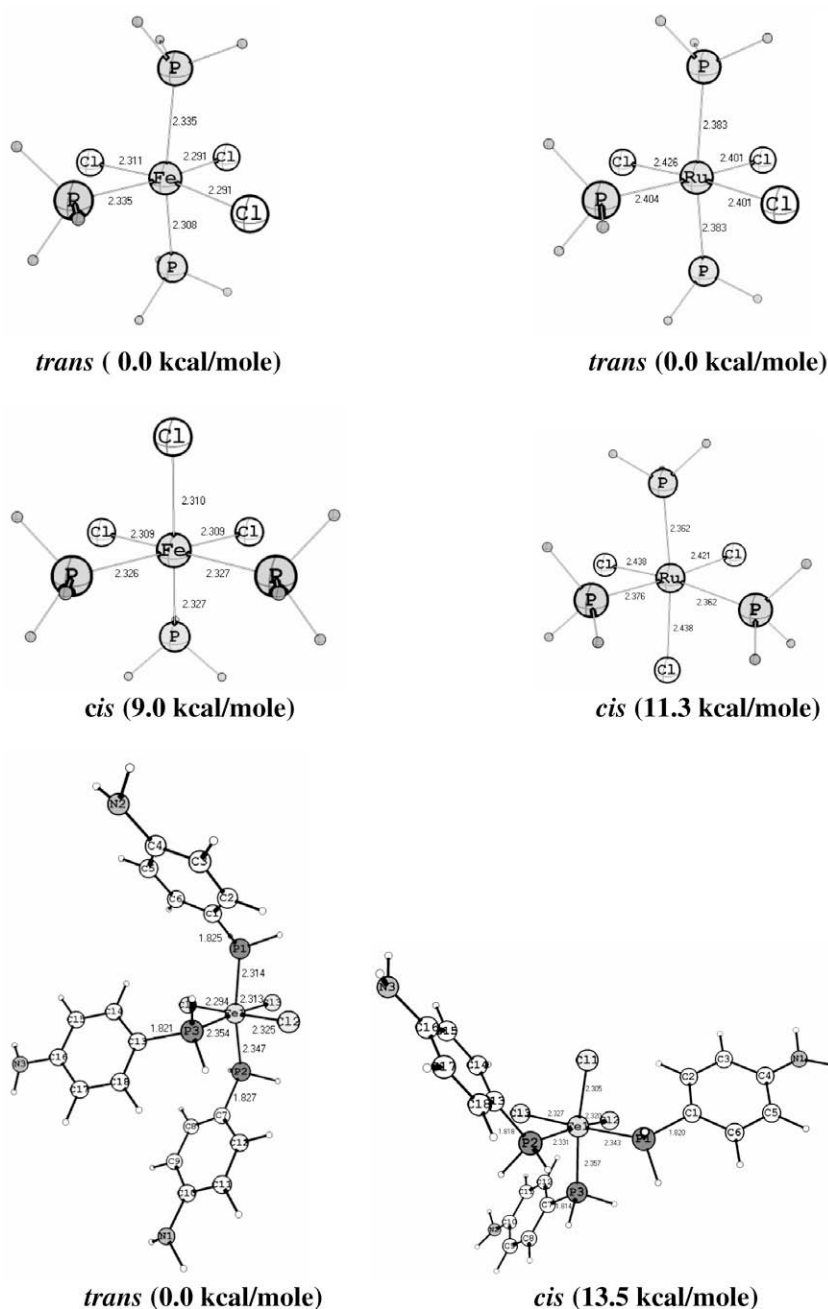


Fig. 7. B3LYP optimized geometry and relative energies of **1** for both Fe and Ru with important bond lengths (in Å). The optimized structure used for computation of UV–Vis spectra of **1** is given at the bottom (**1-trans**).

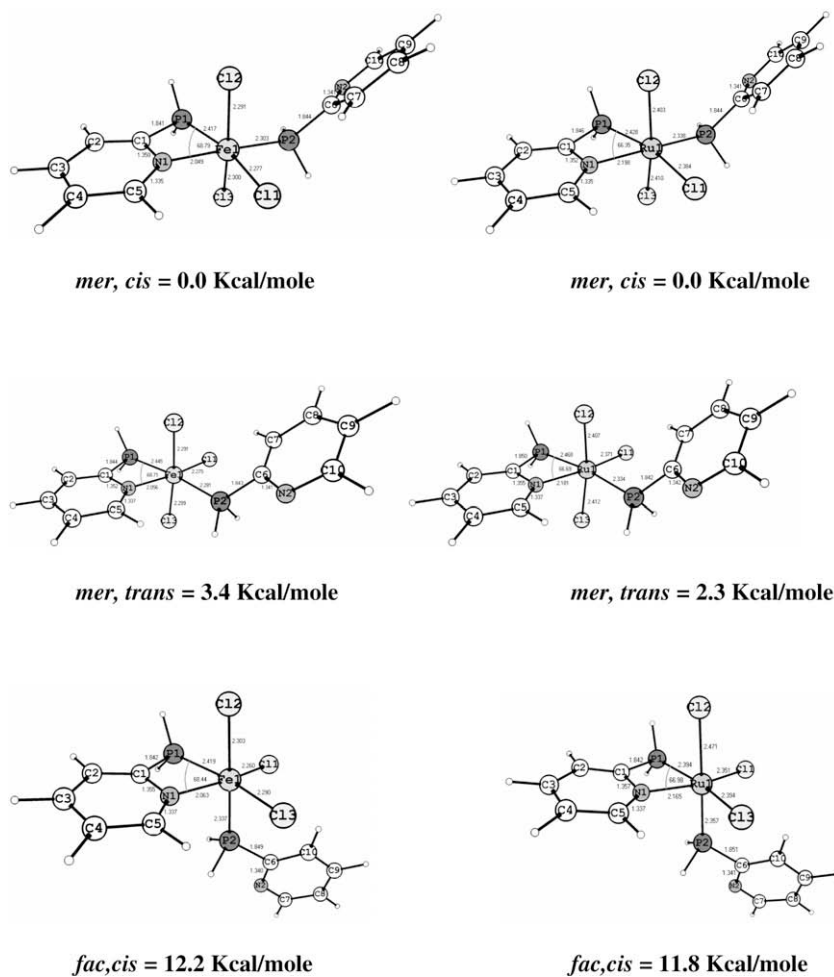


Fig. 8. B3LYP optimized geometry and relative energies of different isomers of **2** for Fe and Ru along with important bond lengths (in Å).

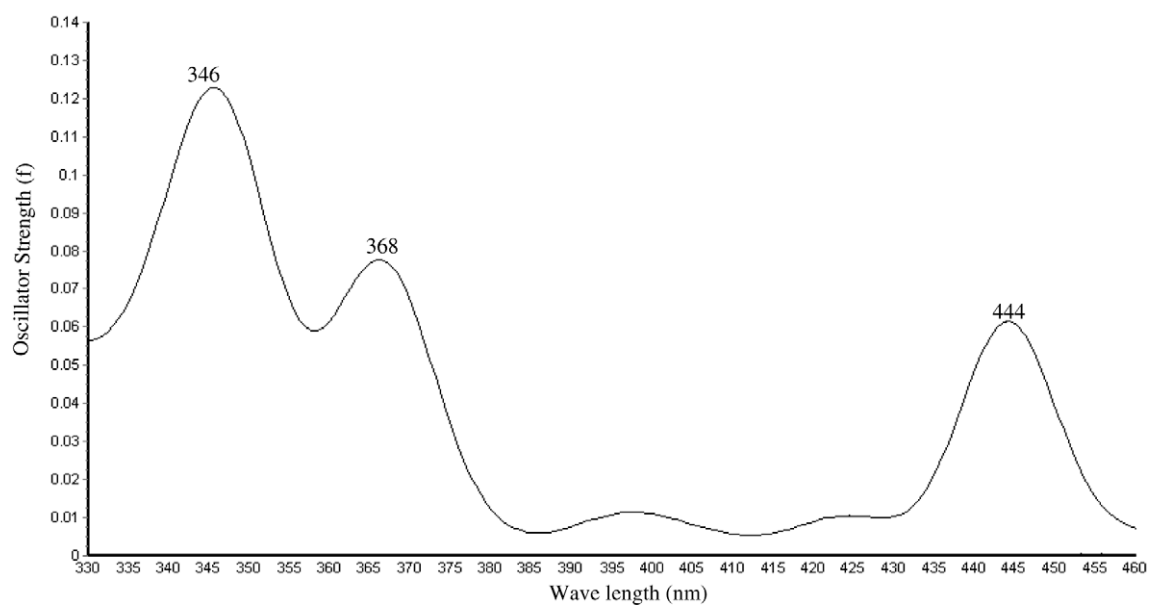


Fig. 9. Simulated electronic spectra of **1** in the gas phase calculated with TDDFT method.

along with the ligand oxidation peak at 1.159 V. Similar type of ligand-based oxidation has also been observed for electrochemical studies on other Fe(III) complexes [1,4a]. It might be important to note here that the electrochemical access for a Fe(III) system to higher valence Fe(IV) state is rather uncommon, but there exists few examples in literature where a low-spin Fe(III) complex with a phosphine [43] or amide based ligand [44] show similar behavior.

#### 4.7. Computational study

Since we could not get any crystal structure for complexes **1** and **2**, we decided to carry out geometry optimization of the com-

plexes and their ruthenium analogs. This is because a ruthenium based complex similar to **2** is known experimentally [23] and thus, comparison can be easily made between similar iron and ruthenium complexes. For **1**, both the *cis* and *trans* isomers and for **2**, all the three possible isomers, viz., *mer,cis*, *mer,trans* and *fac,cis* were considered. The calculated relative energies were similar for both iron and ruthenium (Figs. 7 and 8) and the *trans*, and *mer,cis* isomers were found to be the most stable geometry of **1** and **2**, respectively. Thus, the computational results corroborate the experimental findings that *trans* and *mer,cis* are the most likely geometry of **1** and **2**, respectively. For **2**, the *fac,cis* structure was found to be the least stable. However, the energy difference between all the isomers is not very large. To the best of our knowl-

**Table 2**  
Calculated contributions of the main orbitals involved in transitions, excitation energies ( $E/eV$ ), oscillator strengths ( $f$ ), coefficients of the wave function corresponding to a particular transition ( $\phi_C$ ), wave lengths ( $\lambda$  in nm) of complex **1** obtained from the TDDFT calculations together with the experimental results.

	Major orbital contribution	$E$ (eV)	$f$	$\phi_C$	$\lambda_{cal}$ (nm)	$\lambda_{exp}$ (nm)	Character
1	HOMO ( $\pi_{Ph} + n_P + n_{Cl}$ ) $\rightarrow$ LUMO ( $d_{Fe} + n_{Cl}$ ) (82%)	2.43	0.003	0.90	510	503	LMCT
2 <sup>a</sup>	HOMO ( $\pi_{Ph} + n_P + n_{Cl}$ ) $\rightarrow$ LUMO+1 ( $d_{Fe}$ ) (72%)	2.79	0.085	0.85	444		LM
3 <sup>a</sup>	HOMO-2 ( $\pi_{Ph}$ ) $\rightarrow$ LUMO+1 ( $d_{Fe}$ ) (35%)	3.36	0.065	0.59	368		LM
4	HOMO-1 ( $\pi_{Ph} + n_N$ ) $\rightarrow$ LUMO+3 ( $d_{Fe}$ ) (23%)	3.58	0.107	0.48	346	352	LM

<sup>a</sup> No experimental bands are available at these wave lengths.

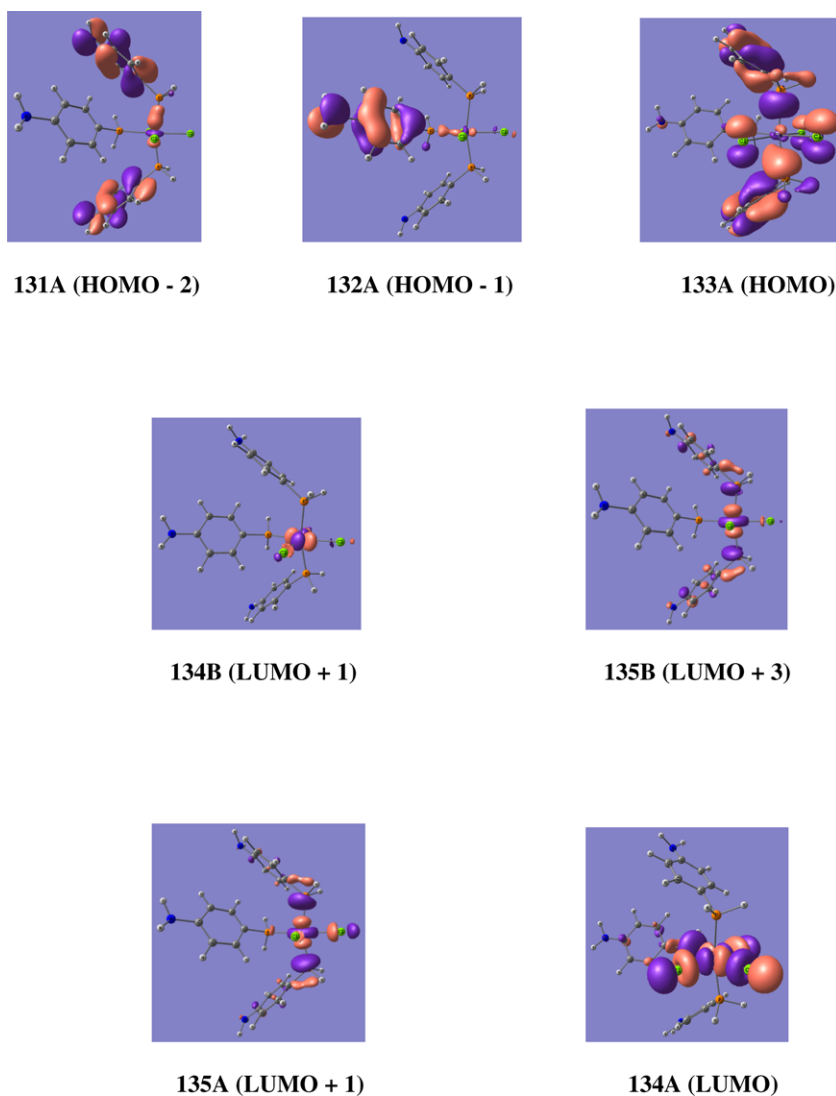


**Fig. 10.** Electron density diagrams of the frontier molecular orbitals involved in the computed absorption transitions of **1** at the B3LYP level of TDDFT theory in the gas phase.

edge, no analogous ruthenium complex of **1** is known in the literature. However, structure **2** is known experimentally for ruthenium which has a *mer,cis* configuration [23] and the computed geometrical parameters of this molecule are in excellent agreement with the X-ray crystal structure. Thus, we will restrict our future discussion to these computed stable geometries only.

#### 4.7.1. Structure of the computed complexes

The *trans* isomer of **1** has a distorted octahedral geometry. The angle between the *trans* ligands are much smaller than 180°. The Cl1–Fe–Cl2, P1–Fe–P2 and P3–Fe–Cl3 angles are 168.9°, 165.3° and 174.8°, respectively. The angles between the *cis* chloride ligands are larger than 90° with values of 95.3° and 94.8° for Cl2–Fe–Cl3 and Cl1–Fe–Cl3, respectively. The computed Fe–Cl bond lengths of 2.294 Å, 2.313 Å and 2.325 Å are comparable to other known complexes of Fe(III) systems [13]. The Fe–P bond *trans* to Cl is longer (2.354 Å) than the other two Fe–P bonds (2.314 Å and 2.347 Å).

The *mer,cis* isomer of **2** is also a six-coordinate complex. It contains two PPh<sub>2</sub>py ligands, one of which acts as a chelating ligand through P and N atoms resulting in a planar four-membered ring comprising Fe, P, C and N. Similar to complex **1**, the calculated Fe–Cl bond lengths of **2** are close to the experimentally determined ones [13]. Out of the two Fe–P bonds, the Fe–P bond *trans* to Cl is longer (2.417 Å) than that *trans* to the N atom of the pyridyl ring (2.303 Å). Similar trends were found for the computed ruthenium counterpart of **2** (Fig. 8) as well as for experimentally reported similar Ru(III) complexes [23]. The Fe–N bond length of 2.049 Å is comparable to other known pyridyl complexes of Fe(III) [13]. Similar to complex **1**, the angle between the *trans* ligands are much smaller than 180° and that between the *cis* chloride ligands are

more than 90°. The *trans* and *cis* angles are 164.1°, 16.5°, 176.2° and 96.6°, 96.5° for P1–Fe–Cl1, Cl2–Fe–Cl3, N1–Fe–P2 and Cl1–Fe–Cl2, Cl1–Fe–Cl3, respectively. The angle between the two *cis* phosphorus atoms is computed to be 109.6° which is in close agreement with that observed for similar experimentally known Ru(III) complexes [13]. The P–Fe–N bite angle of the four-membered metallocycle is found to be 68.8° and is slightly larger than those found for related ruthenium complexes.

#### 4.7.2. Electronic spectra of the complexes

The computed absorption spectra of **1** (Fig. 9) shows two additional bands than the observed spectra. Three of these bands are obtained at 444 nm, 368 nm and 346 nm with large oscillator strength ( $f = 0.085, 0.065$  and  $0.107$ , respectively). There is also a very weak and broad band at 510 nm with very small oscillator strength ( $f = 0.003$ ). The calculated excitation energies, oscillator strengths and the major molecular orbitals involved in these transitions along with the experimental values are given in Table 2 and the frontier molecular orbitals involved in different absorption transition of complex **1** are displayed in Fig. 10.

As seen from Table 2, the lower energy transition at 510 nm originates mainly from the HOMO → LUMO transition and this transition has the largest coefficient (0.90) in the TDDFT wave function. The electron density in HOMO is distributed between the phenyl ligands, Cl and P atoms, but that in LUMO is localized on the Cl and Fe atoms in an antibonding manner. Considering Table 2 and Fig. 10, we attribute the 510 nm absorption to LMCT (ligand to metal charge transfer) which is in tune with the experimental results. The next intense band at 444 nm originates mainly from the HOMO → LUMO+1 transition and this transition has the largest coefficient (0.85) in the TDDFT wave function. The

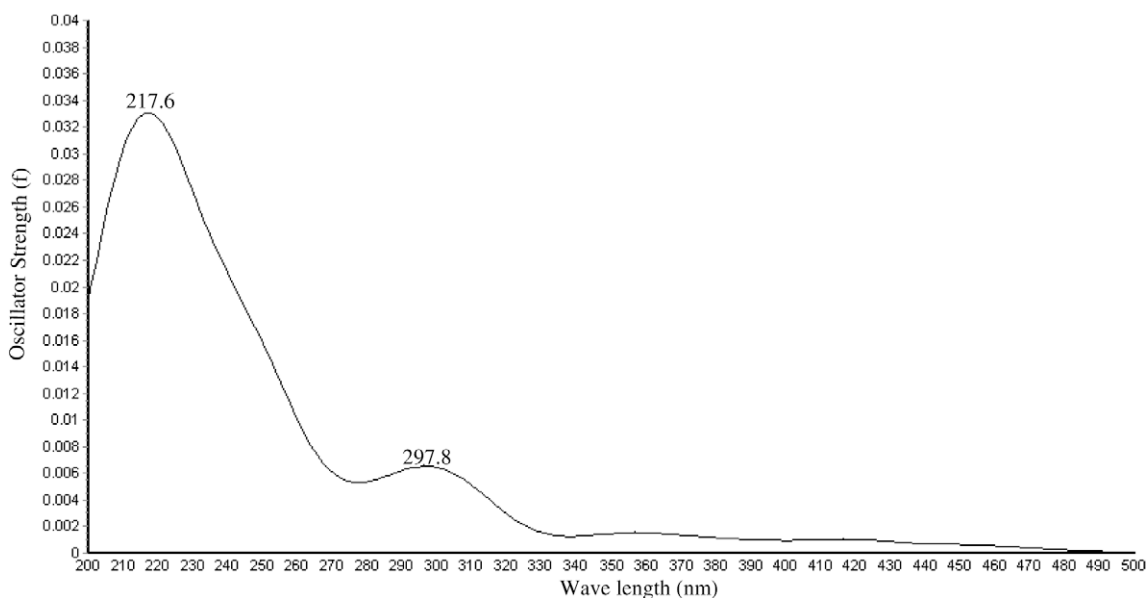


Fig. 11. Simulated electronic spectra of **2** in the gas phase calculated with TDDFT method.

Table 3

Calculated contributions of the main orbitals involved in transitions, excitation energies ( $E$ /eV), oscillator strengths ( $f$ ), coefficients of the wave function corresponding to a particular transition ( $\phi_c$ ), wave lengths ( $\lambda$  in nm) of complex **2** obtained from the TDDFT calculations together with the experimental results.

	Major orbital contribution	$E$ , (eV)	$f$	$\phi_c$	$\lambda_{cal}$ (nm)	$\lambda_{exp}$ (nm)	Character
1	HOMO ( $n_{Cl}$ ) → LUMO ( $d_{Fe} + n_{Cl}$ ) (37%)	2.44	0.0004	0.60	508	526	LMCT
2	HOMO-3( $n_{Cl}$ ) → LUMO+1( $d_{Fe} + n_p + n_{Cl}$ ) (24%) HOMO-1 ( $n_{Cl}$ ) → LUMO+1 ( $d_{Fe} + n_p$ ) (21%)	2.96	0.0154	0.49 0.46	418	403	LMCT
3	HOMO-5 ( $n_{Cl}$ ) → LUMO+2 ( $\pi^*_{py}$ ) (62%)	4.16	0.004	0.78	297.8	297	$\pi$ - $\pi^*$
4	HOMO-12 ( $\pi_{py}$ ) → LUMO+2 ( $\pi^*_{py}$ ) (11%)	5.70	0.036	0.33	217.6	228	$\pi$ - $\pi^*$

LUMO+1 orbital is concentrated on Fe and P atoms. By looking at Fig. 10, this transition can be assigned to  $\pi_{\text{ph}} + n_{\text{P}} \rightarrow d_{\text{Fe}}$  transition. The major transition contribution to the band at 368 nm comes from HOMO-2  $\rightarrow$  LUMO+1 which has a coefficient of 0.59 in the wave function. The HOMO-2 orbital chiefly composed of  $\pi$  orbitals of phenyl rings with only a minor contribution coming in from the N lone pair (Fig. 10) and thus, this transition can be assigned to  $\pi_{\text{ph}} \rightarrow d_{\text{Fe}}$  transition. The most intense band at 346 nm arises mainly from the HOMO-1  $\rightarrow$  LUMO+3 transitions having a coefficient of 0.48 in computed wave function. The HOMO-1 is predominantly a phenyl  $\pi$  orbital with some contribution from the lone pair on N whereas the LUMO+3 is a metal based orbital. Thus, this transition can be attributed to the  $\pi_{\text{ph}} + n_{\text{N}} \rightarrow d_{\text{Fe}}$  transition.

The calculated absorption spectrum of complex **2** is shown in Fig. 11. It features a shoulder at 297 nm ( $f = 0.004$ ) and a moderately intense band at 217.6 nm ( $f = 0.036$ ). In addition, there are two more weak and broad band at 508 ( $f = 0.0004$ ) and 418 nm ( $f = 0.0154$ ). The calculated excitation energies, oscillator strengths and the major molecular orbitals involved in these transitions along with the experimental values are given in Table 3 and the frontier molecular orbitals involved in different absorption transition of complex **2** are displayed in Fig. 12.

The origin of the lowest energy transition at 508 nm lies mainly in HOMO  $\rightarrow$  LUMO transition having a coefficient of 0.60 in the TDDFT wave function. The HOMO is largely localized on Cl and the LUMO is a combination of metal d-orbital and Cl p-orbital. A careful examination of Table 3 and Fig. 12 reveals that this transition can be attributed to ligand ( $n_{\text{Cl}}$ ) to metal ( $d_{\text{Fe}} + n_{\text{Cl}}$ ) charge transfer (LMCT). The band at 418 nm involves transition from HOMO-3 and HOMO-1 to LUMO+1 having coefficients of 0.49 and 0.46, respectively in the wave function. Both HOMO-1 and HOMO-3 are concentrated on Cl atoms whereas the LUMO+1 has contribution from metal, Cl and the lone pair on P atoms. Taken together, this band can be assigned to ligand ( $n_{\text{Cl}}$ ) to metal ( $d_{\text{Fe}} + n_{\text{P}} + n_{\text{Cl}}$ ) charge transfer (LMCT) transitions (Table 3 and Fig. 12). The shoulder at 297.8 nm originates mostly from HOMO-5  $\rightarrow$  LUMO+2 transition having a coefficient of 0.78 in the wave function. A look at Fig. 12 clearly shows that HOMO-5 and LUMO+2 corresponds to the non-bonding orbital on Cl and  $\pi^*$  orbital of the chelating pyridine ligand, respectively. Thus, this transition can be considered as an  $n \rightarrow \pi^*$  transition. Out of all the absorption band of complex **2**, the most intense band at 217.6 nm having a wave function coefficient of 0.33 arises from HOMO-12  $\rightarrow$  LUMO+2 transition. The lower lying HOMO-12 is

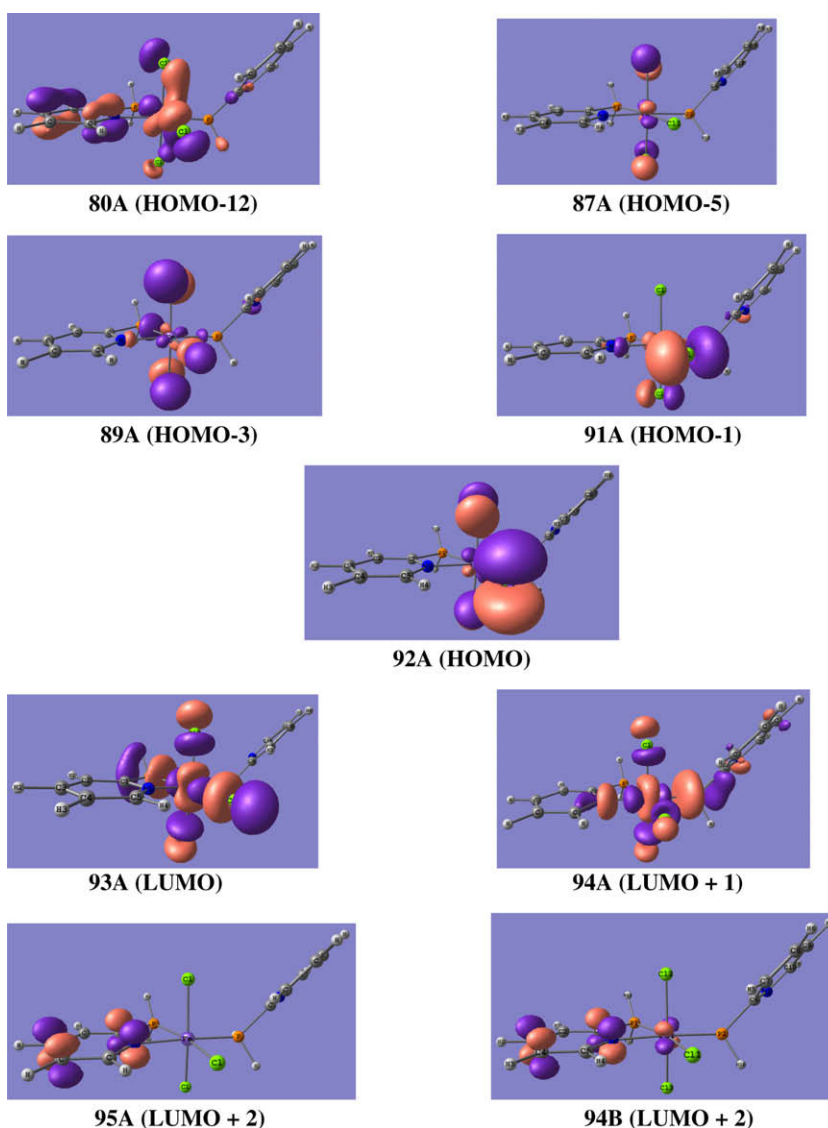


Fig. 12. Electron density plots of the frontier molecular orbitals involved in the computed absorption transitions of **2** at the B3LYP level of TDDFT theory in the gas phase.

mostly a filled  $\pi$  bonding orbital centered on the chelated pyridine ring and the LUMO+2 belongs to the  $\pi^*$  orbital of the same ligand and therefore, this band can be attributed to  $\pi \rightarrow \pi^*$  transition. All the calculated bands are in close agreement with the experimentally observed ones.

## 5. Conclusion

Two new mononuclear, non-heme Fe(III) complexes with two hemilabile P,N donor ligands were synthesized and characterized by different experimental techniques. EPR and magnetic studies revealed that the complexes are low-spin at room temperature and the spin state does not change even after lowering the temperature. In the absence of any crystal structure, theoretical calculations were performed on all the possible isomers of complexes **1** and **2** and they were compared with similar complexes of ruthenium for which X-ray structure was available. The calculations predict a *trans*- and *mer,cis*-geometry for complexes **1** and **2**, respectively which is in conformity with those derived from the IR spectral analysis. The computationally simulated UV–Vis spectra and their spectral assignments are in excellent agreement with the experimentally observed bands.

## Acknowledgements

The authors P.D. and A.K.P are grateful to the Department of Science and Technology, New Delhi, for financial support (SR/FTP/CS-119/2005 and SR/FTP/CS-85/2005). The services of SAIF, IIT, Bombay, SAIF, CDRI, Lucknow and IIT, Kanpur were gratefully acknowledge for recording ESR, Mass and Magnetic analysis, respectively.

## Appendix A. Supplementary material

Supplementary data associated with this article can be found, in the online version, at doi:10.1016/j.ica.2009.08.006.

## References

- [1] T. Beissel, K.S. Burger, G. Voigt, K. Wieghardt, C. Butzlaff, A.X. Trautwein, *Inorg. Chem.* 32 (1993) 124.
- [2] S.C. Shoner, D. Barnhart, J.A. Kovacs, *Inorg. Chem.* 34 (1995) 4517.
- [3] A.L. Nivorozhkin, A.I. Uraev, G.I. Bondarenko, A.S. Antsyshkina, V.P. Kurbatov, A.D. Garnovskii, C.I. Turta, N.D. Brashoveanu, *Chem. Commun.* (1997) 1711.
- [4] (a) J.C. Noveron, R. Herradora, M.M. Olmstead, P.K. Mascharak, *Inorg. Chim. Acta* 285 (1999) 269; (b) J.C. Noveron, M.M. Olmstead, P.K. Mascharak, *J. Am. Chem. Soc.* 123 (2001) 3247.
- [5] E.W.Y. Tido, G.O.R.A. van Ekenstein, A. Meetsma, P.J. van Koningsbruggen, *Inorg. Chem.* 47 (2008) 143.
- [6] F. Li, M. Wang, C. Ma, A. Gao, H. Chen, L. Sun, *Dalton Trans.* (2006) 2427.
- [7] N.M.F. Carvalho, O.A.C. Antunes, A. Horn Jr., *Dalton Trans.* (2007) 1023.
- [8] M. Pascaly, M. Duda, F. Schweppe, K. Zurlinden, F.K. Muller, B. Krebs, *J. Chem. Soc., Dalton Trans.* (2001) 828.
- [9] R. Mayilmurugan, E. Suresh, M. Palaniandavar, *Inorg. Chem.* 47 (2008) 6645.
- [10] M. Palaniandavar, R. Mayilmurugan, C. R. *Chimie* 10 (2007) 366.
- [11] N.M.F. Carvalho, A. Horn Jr., A.J. Bortoluzzi, V. Drago, O.A. Antunes, *Inorg. Chim. Acta* 359 (2006) 90.
- [12] A. Hazell, C.J. McKenzie, L.P. Nielsen, S. Schindler, M. Weitzer, *J. Chem. Soc., Dalton Trans.* (2002) 310.
- [13] D. Mandon, A. Nopper, T. Litrol, S. Goetz, *Inorg. Chem.* 40 (2001) 4803.
- [14] O. Rotthaus, S.L. Roy, A. Thomas, K.M. Barkigia, I. Artaud, *Inorg. Chim. Acta* 357 (2004) 2211.
- [15] M.C. Rodriguez, F. Lambert, I.M. Badarau, M. Cesario, J. Guilhem, B. Keita, L. Nadjio, *Inorg. Chem.* 36 (1997) 3525.
- [16] M.C. Rodriguez, I.M. Badarau, M. Cesario, J. Guilhem, B. Keita, L. Nadjio, *Inorg. Chem.* 35 (1996) 7840.
- [17] F.A. Cotton, G. Wilkinson, *Advanced Inorganic Chemistry*, 4th ed., Wiley, New York, 1980. pp. 648, 761.
- [18] Y. Sugiyra, J. Kuwahara, T. Nagasawa, H. Yamada, *J. Am. Chem. Soc.* 109 (1987) 5848.
- [19] A.K. Patra, M.M. Olmstead, P.K. Mascharak, *Inorg. Chem.* 41 (2002) 5403.
- [20] A. Hazell, K.B. Jensen, C.J. McKenzie, H. Toftlund, *Inorg. Chem.* 33 (1994) 3127.
- [21] S.S. Massoud, K.T. Broussard, F.A. Mautner, R. Vicente, M.K. Saha, I. Bernal, *Inorg. Chim. Acta* 361 (2008) 123.
- [22] P. Das, J.F. Capon, F. Gloaguen, F.Y. Petillon, P. Schollhammer, J. Talarmin, K.W. Muir, *Inorg. Chem.* 43 (2004) 8203.
- [23] K.W. Hermanowicz, Z. Ciunik, A. Kochel, *Inorg. Chem.* 45 (2006) 3369.
- [24] H.B. Song, Z.Z. Zhang, T.C.W. Mak, *Inorg. Chem.* 40 (2001) 5928.
- [25] S.L. Li, T.C.W. Mak, Z.Z. Zhang, *J. Chem. Soc., Dalton Trans.* (1996) 3475.
- [26] E.C. Carson, S.J. Lippard, *Inorg. Chem.* 45 (2006) 837.
- [27] E.C. Carson, S.J. Lippard, *J. Am. Chem. Soc.* 126 (2004) 3412.
- [28] J.D. Walker, R. Poli, *Inorg. Chem.* 28 (1989) 1793.
- [29] W. Baratta, C. Mealli, E. Herdtweck, A. Lenco, S.A. Mason, P. Rigo, *J. Am. Chem. Soc.* 126 (2004) 5549.
- [30] A.D. Becke, *J. Chem. Phys.* 98 (1993) 5648.
- [31] A.D. Becke, *Phys. Rev. A* 38 (1988) 2398.
- [32] C. Lee, W. Yang, R.G. Parr, *Phys. Rev. B* 37 (1988) 785.
- [33] P.J. Hay, W.R. Wadt, *J. Chem. Phys.* 82 (1985) 270.
- [34] W.R. Wadt, P.J. Hay, *J. Chem. Phys.* 82 (1985) 284.
- [35] P.J. Hay, W.R. Wadt, *J. Chem. Phys.* 82 (1985) 299.
- [36] M.J. Frisch, G.W. Trucks, H.B. Schlegel, G.E. Scuseria, M.A. Robb, J.R. Cheeseman, J.A. Montgomery Jr., T. Vreven, K.N. Kudin, J.C. Burant, J.M. Millam, S.S. Iyengar, J. Tomasi, V. Barone, B. Mennucci, M. Cossi, G. Scalmani, N. Rega, G.A. Petersson, H. Nakatsuji, M. Hada, M. Ehara, K. Toyota, R. Fukuda, J. Hasegawa, M. Ishida, T. Nakajima, Y. Honda, O. Kitao, H. Nakai, M. Klene, X. Li, J.E. Knox, H.P. Hratchian, J.B. Cross, V. Bakken, C. Adamo, J. Jaramillo, R. Gomperts, R.E. Stratmann, O. Yazyev, A.J. Austin, R. Cammi, C. Pomelli, J.W. Ochterski, P.Y. Ayala, K. Morokuma, G.A. Voth, P. Salvador, J.J. Dannenberg, V.G. Zakrzewski, S. Dapprich, A.D. Daniels, M.C. Strain, O. Farkas, D.K. Malick, A.D. Rabuck, K. Raghavachari, J.B. Foresman, J.V. Ortiz, Q. Cui, A.G. Baboul, S. Clifford, J. Cioslowski, B.B. Stefanov, G. Liu, A. Liashenko, P. Piskorz, I. Komaromi, R.L. Martin, D.J. Fox, T. Keith, M.A. Al-Laham, C.Y. Peng, A. Nanayakkara, M. Challacombe, P.M.W. Gill, B. Johnson, W. Chen, M.W. Wong, C. Gonzalez, J.A. Pople, *GAUSSIAN 03*, Revision C.02, Gaussian, Inc., Wallingford, CT, 2004.
- [37] R.E. Stratmann, G.E. Scuseria, M.J. Frisch, *J. Chem. Phys.* 109 (1998) 8218.
- [38] R. Bauernschmitt, R. Ahlrichs, *Chem. Phys. Lett.* 454 (1996) 256.
- [39] M.E. Casida, C. Jamorski, K.C. Casida, D.R. Salahub, *J. Chem. Phys.* 108 (1998) 4439.
- [40] J.R. Dilworth, S.D. Howe, A.J. Hutson, J.R. Miller, J. Silver, R.M. Thompson, M. Harman, M.B. Hursthouse, *J. Chem. Soc., Dalton Trans.* (1994) 3553.
- [41] K. Nakamoto, *Infrared Spectra of Inorganic and Coordination Compounds*, 2nd ed., Wiley, New York, 1970. p. 205.
- [42] J.C. Daran, Y. Jeanin, L.M. Martin, *Inorg. Chem.* 19 (1980) 2935.
- [43] Piero Zanello, *Inorganic Electrochemistry Theory, Practice and Application*, Royal Science Society, Cambridge, 2003 (p. 211).
- [44] E. Pardo, F. Lloret, R. Carrasco, M.C. Munoz, T.T. Sanchez, R.R. Garcia, *Inorg. Chim. Acta* 357 (2004) 2713.